CIVIL AND ENVIRONMENTAL ENGINEERING REPORTS

No. 1 2005

NUMERICAL HOMOGENIZATION OF ELASTIC BRICK MASONRY

Mieczysław KUCZMA, Krystyna WYBRANOWSKA
University of Zielona Góra, prof. Z. Szafrana St. 2,
65-516 Zielona Góra, Poland

The paper is concerned with a numerical homogenization technique for determination of effective material properties of brick masonry in the elastic range. The homogenization problem is posed in the plane state of stress. The corresponding boundary value problem on a representative cell is discretized by the finite element method. The quadrilateral finite element with four nodes and eight degrees of freedom is applied and our own computer program is developed. The homogenization technique allows one to determine for masonry, which is an inhomogeneous two-phase composite medium, an equivalent homogeneous orthotropic material characterized by five material constants. The homogenized material constants can further be used in an analysis of large-scale masonry structures. The obtained results of numerical simulations are compared with predictions of the value of elastic modulus for masonry by other researches, and qualitative agreement can be observed.

Key words: masonry, homogenization technique, finite element method.

1. INTRODUCTION

Brick masonry is a proved composite material formed by a regular connection of bricks by means of mortar joints. Mechanical properties of masonry depend upon the mechanical properties of its components and upon the distribution pattern of this two component system. In the mathematical modelling of masonry, one can also introduce a third element – the interface between bricks and mortar. When treated as a structural material working in plane state conditions, masonry is by its nature an orthotropic material. The complex mechanical behaviour of masonry has led engineers in the past to relay heavily on laboratory

ISBN 83-89712-71-7

test and empirical formulae for the design of masonry structures [3, 5, 6, 9, 11, 12]. Although this approach has resulted in safe designs, it gives very little insight into the behaviour of the material under stress. Now, with the advent of powerful digital computers and sophisticated methods of analysis, a better understanding of the load-bearing response of masonry can be gained by means of numerical simulation [2, 10].

In the mathematical modelling of masonry one can generally distinguish two classes of models [1, 2, 4, 7, 8]: *heterogeneous models* and *homogeneous models*. In heterogeneous models, for each component a suitable (usually isotropic) constitutive law is used and masonry (a masonry structure) is analysed by discretisation of each phase with finite elements separately. In homogeneous models, use is made of the notion of an equivalent homogeneous continuum, the properties of which can be obtained in laboratory tests on masonry specimens or by a theoretical homogenisation procedure where the notion of a representative volume element is applied. Within each class of models, there exist further splits into subclasses due to different types of constitutive laws and effects account for (elasticity, plasticity, damage, failure, unilateral constraints). Although being accurate and in many circumstances unavoidable, the heterogeneous models are not suitable for analysis of real masonry structures because they lead to large computational costs and storage requirements. On the contrary, although not capable to reproduce precisely local effects, homogeneous models are very useful in the analysis of behaviour of large-scale masonry structures.

Our main aim in this paper is to determine the equivalent elastic parameters for brick masonry in the elastic range of response. Our analysis is based on a numerical homogenization technique and will be performed on a 2D representative volume element (RVE, here denoted by REO). We have solved some relevant boundary value problems for the REO by making use of the finite element method and developing our own computer program. Finally, we have obtained numerical values of the following parameters for an equivalent orthotropic material: $\overline{E}_x$, $\overline{E}_y$ - Young's moduli, $\overline{\nu}_x$, $\overline{\nu}_y$ – Poisson's ratios, $\overline{G}$ - Kirchhoff's modulus. These parameters can be treated as effective elastic properties of masonry and can be utilized in modelling of large-scale masonry structures.

2. REPRESENTATIVE CELLS

Masonry can be considered as a periodic two-phase composite material. In this study, a typical cell of masonry is called a representative element (REO), cf. fig.1. For brick masonry under consideration we have selected four representative cells: REO_I and REO_II and their larger counterparts MUR_I and

MUR_II, shown in fig. 2 with given characteristic dimensions in cm. The behaviour of these masonry units will be modelled numerically by dividing the area occupied by each component material into finite elements separately and solving some boundary value problems.

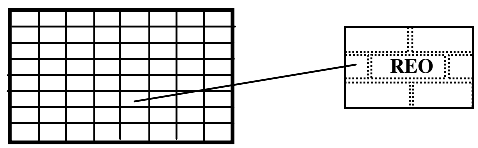

Fig. 1. Masonry as a periodic composite material

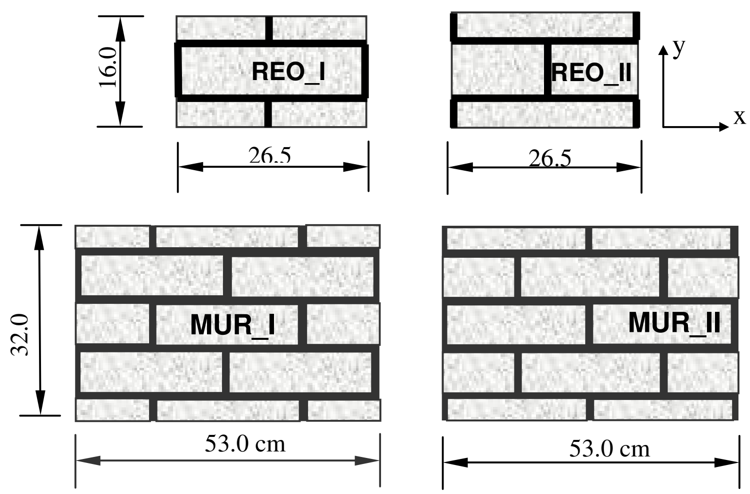

Fig. 2. Representative cells used

Let $\boldsymbol{\sigma}$ and $\boldsymbol{\varepsilon}$ denote the stress and the strain tensor, respectively. Having solved the displacement boundary value problem on a cell and having determined the corresponding stress $\boldsymbol{\sigma}$ and strain $\boldsymbol{\varepsilon}$, we can calculate their average values, $\overline{\boldsymbol{\sigma}}$ and $\overline{\boldsymbol{\varepsilon}}$, as follows

$$\overline{\boldsymbol{\sigma}} = \frac{1}{|\Omega|}\int_{\Omega} \boldsymbol{\sigma}\, d\Omega, \qquad \overline{\boldsymbol{\varepsilon}} = \frac{1}{|\Omega|}\int_{\Omega} \boldsymbol{\varepsilon}\, d\Omega \tag{1}$$

wherein $|\Omega|$ stands for the area of cell.

The mutual relationship of $\boldsymbol{\sigma}$ and $\boldsymbol{\varepsilon}$ depends on the constitution of each component material and is defined next.

3. CONSTITUTIVE EQUATIONS

In the present study, bricks and mortar are modelled as isotropic linearly elastic materials. Furthermore, we consider the case that these masonry materials are in the plane state of stress and have the following constitutive relation between $\boldsymbol{\sigma}$ and $\boldsymbol{\varepsilon}$ written in matrix form,

$$\begin{bmatrix} \sigma_x \\ \sigma_y \\ \tau_{xy} \end{bmatrix} = \frac{E}{1-\nu^2} \begin{bmatrix} 1 & \nu & 0 \\ \nu & 1 & 0 \\ 0 & 0 & \frac{1-\nu}{2} \end{bmatrix} \begin{bmatrix} \varepsilon_x \\ \varepsilon_y \\ \gamma_{xy} \end{bmatrix} \tag{2}$$

in which E and ν are Young's modulus and Poisson's number applied for each material individually.

The constitutive equations for an orthotropic material under plane stress condition are characterised by five independent material parameters: $E_x, E_y, \nu_x, \nu_y, G$ and may be written as follows

$$\begin{bmatrix} \sigma_x \\ \sigma_y \\ \tau_{xy} \end{bmatrix} = \begin{bmatrix} \frac{E_x}{1-\nu_x\nu_y} & \frac{E_x\nu_y}{1-\nu_x\nu_y} & 0 \\ \frac{E_y\nu_x}{1-\nu_x\nu_y} & \frac{E_y}{1-\nu_x\nu_y} & 0 \\ 0 & 0 & G \end{bmatrix} \begin{bmatrix} \varepsilon_x \\ \varepsilon_y \\ \gamma_{xy} \end{bmatrix} \tag{3}$$

Based on equations (3) and a set of numerical solutions obtained for particular boundary conditions, we shall calculate effective properties of brick masonry in the sequell. The numerical solutions are determined by the finite element method (FEM) [10].

4. SOLUTION METHOD AND NUMERICAL EXAMPLES

The purpose of this section is twofold. First, we briefly recall notations and basic relations of the finite element method we applied to the 2D elasticity problem under study. Then, we wish to present some of the obtained results of numerical simulations.

We have discretized the problem using the quadrilateral finite element with four nodes and 8 degrees of freedom (DOF) which are nodal displacements

$\mathbf{q}_i = \{u_i, v_i\}$, $i = 1,2,3,4$, see fig. 3. Let $\mathbf{u} = \{u, v\}$ $\mathbf{K}^e \mathbf{q}^e = \mathbf{f}^e$ denote the displacement vector with horizontal $u = u(x, y)$ and vertical $v = v(x, y)$ components which are functions of coordinates $(x, y) \in \Omega$. Within a typical finite element *e* occupying the region $\Omega^e \subset \Omega$, the displacement field $\mathbf{u}^e = \mathbf{u}^e(x, y)$ can be expressed as

$$\mathbf{u}^e(x, y) = \mathbf{N}(x, y)\,\mathbf{q}^e \tag{4}$$

where $\mathbf{q}^e = \{\mathbf{q}_1, \mathbf{q}_2, \mathbf{q}_3, \mathbf{q}_4\}$ is the vector of nodal displacements of element *e*, while $\mathbf{N}$ is the matrix of shape functions whose entries, for the considered finite element, are assumed functions of the form $\alpha + \beta x + \gamma y + \eta x y$.

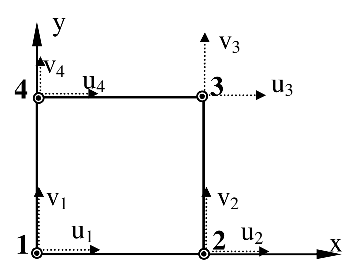

Fig. 3 Finite element Q4 used in numerical analysis

In terms of $\mathbf{q}^e$ we can also express the stresses and strains in element *e*:

$$\boldsymbol{\varepsilon}^e = \mathbf{B}\mathbf{q}^e = \partial \mathbf{N}\mathbf{q}^e \tag{5}$$

$$\sigma^e = \mathbf{D}\varepsilon^e = \mathbf{D}\mathbf{B}\mathbf{q}^e \tag{6}$$

where ∂ is the matrix differential operator generated by the geometrical relations $\varepsilon_{ij} = (\partial u_i / \partial x_j + \partial u_j / \partial x_i)/2$, where standard index notation is used, and $\mathbf{D}$ is the matrix of elasticities as defined in (2) or (3).

The equations of static equilibrium for element *e* can be written as the matrix equation

$$\mathbf{K}^e \mathbf{q}^e = \mathbf{f}^e \tag{7}$$

in which $\mathbf{K}^e$ is the stiffness matrix of element *e* and $\mathbf{f}^e$ is a vector of elemental nodal forces given by

$$\mathbf{K}^e = t \int_{\Omega^e} \mathbf{B}^T \mathbf{D} \mathbf{B} \, d\Omega \tag{8}$$

$$\mathbf{f}^e = \int_{\Omega^e} \mathbf{N}^T \mathbf{g} \, d\Omega \tag{9}$$

with t denoting the thickness of masonry and $\mathbf{g} = (g_x, g_y)$ the vector of loading.

Closed formulae for entries K_{ij} of the elemental stiffness matrix $\mathbf{K}^e$ are listed at the end of paper in Appendix.

By aggregation of all elemental contributions $\mathbf{K}^e$ and $\mathbf{f}^e$ we finally arrive at the global equilibrium equations for a cell as a whole [10],

$$\mathbf{K}\,\mathbf{q} = \mathbf{f} \tag{10}$$

in which **K** is the global stiffness matrix and **f** is the global vector of nodal loads. Having accounted for the boundary conditions, we solve the system of linear equations (10) for the global vector of nodal displacements **q**.

Now, let us pass to numerical simulations of the behaviour of masonry that will be carried out on selected representative cells. For the representative cells REO_I and REO_II we have used three meshes, cf. figs. 4-6:

- S1: 210 elements, 242 nodes, 484 DOF,
- S2: 760 elements, 819 nodes, 1638 DOF,
- S3: 1456 elements, 1537 nodes, 3074 DOF,

and one mesh for cells MUR_I and MUR_II:

- M1:1056 elements, 1125 nodes, 2250 DOF.

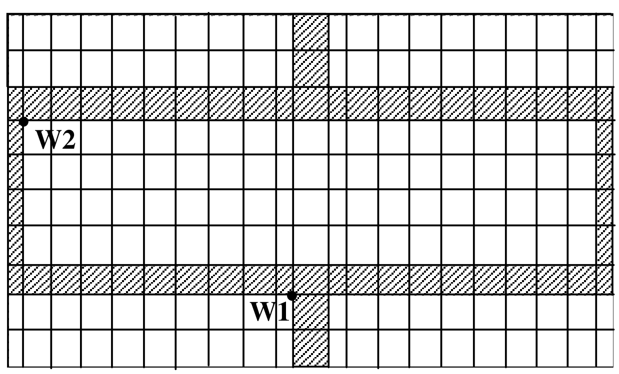

Fig. 4. REO_I, Mesh S1: 210 elements, 242 nodes, 484 DOF

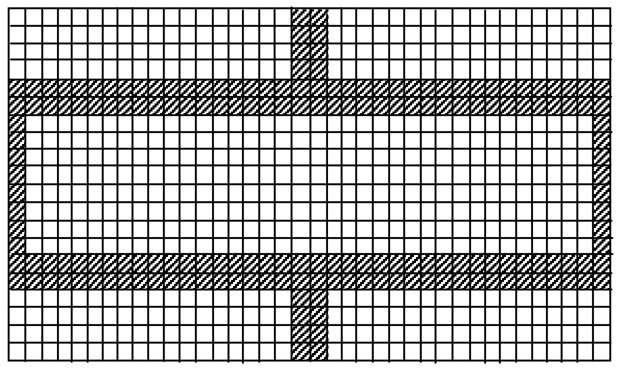

Fig. 5. REO_I, Mesh S2: 760 elements, 819 nodes, 1638 DOF

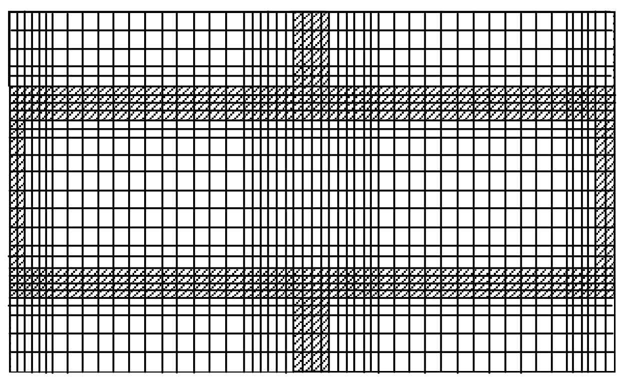

Fig. 6. REO_I, Mesh S3: 1456 elements, 1537 nodes, 3074 DOF

As can be seen, bricks and mortar joints are discretized individually. The dimensions of the brick are 25 x 12 x 6.5 cm and the assumed thickness of (bed and head) mortar joints is 1.5 cm. The material parameters for brick and mortar were taken from literature [1], [4] and are summarized in Table 1. On the surface of REO_I and REO_II we have selected two characteristic points w1 and w2, at which we will observe changes in displacements and stresses for various cases of loads and meshes.

Table 1. Material parameters for brick and mortar

Material	f_c	$E_x = E_y$	$v_x = v_y$	$G=E/2(1+v)$
Brick	≈ 52	11000	0,20	4580
Mortar	≈ 4,0	2200	0,25	880

In table 1 we denote: f_c – compressive strength [MPa], E_x, E_y – Young's modulus [MPa], G – Kirchhoff's modulus [MPa], v_x, v_y –Poisson's ratios.

We have considered three load cases of imposed boundary displacements, see fig. 7, with the following induced averaged strains:

- load case 1 – horizontal compression: $u \neq 0$, $v = 0$; $\bar{\varepsilon}_x \neq 0$, $\bar{\varepsilon}_y = 0$, $\bar{\gamma}_{xy} = 0$,
- load case 2 – vertical compression: $v \neq 0$, $u = 0$; $\bar{\varepsilon}_y \neq 0, \bar{\varepsilon}_x = 0$, $\bar{\gamma}_{xy} = 0$,
- load case 3 – horizontal shear: $u \neq 0$, $v = 0$; $\bar{\varepsilon}_x = 0$, $\bar{\varepsilon}_y = 0$, $\bar{\gamma}_{xy} \neq 0$.

It is worth noticing in passing that the enforced horizontal and vertical boundary displacements generate displacement fields that satisfy uniform strain boundary conditions.

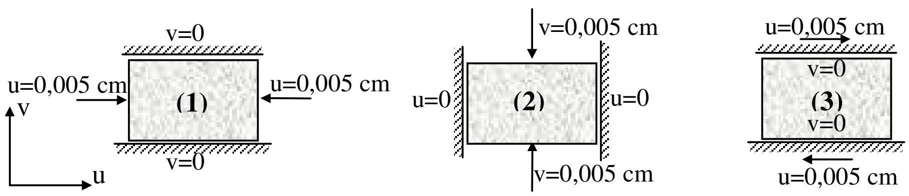

Fig.7. Load cases of imposed boundary displacements: (1) – horizontal compression, (2) – vertical compression, (3) – horizontal shear

For all the indicated representative masonry cells REO and MUR and finite element meshes we have simulated the three load cases and the obtained distributions of stresses σ_x, σ_y, τ_{xy} and strains ε_x, ε_y, γ_{xy} were used to calculate averaged stresses and strains in the corresponding cells and then the effective material parameters. It should be noted that the numerical results obtained for REO_I, REO_II and MUR_I, MUR_II for similar meshes are actually the same. Hence we illustrate graphically the obtained results only for cell REO_I and load case 2.

Figs. 8 and 9 show influence of the coarseness of finite element mesh on values of displacements and stresses at point w1 and w2 which are located at interface mortar-brick corners, cf. fig. 4. As one could expect, the biggest relative changes are in shear stresses τ_{xy} .

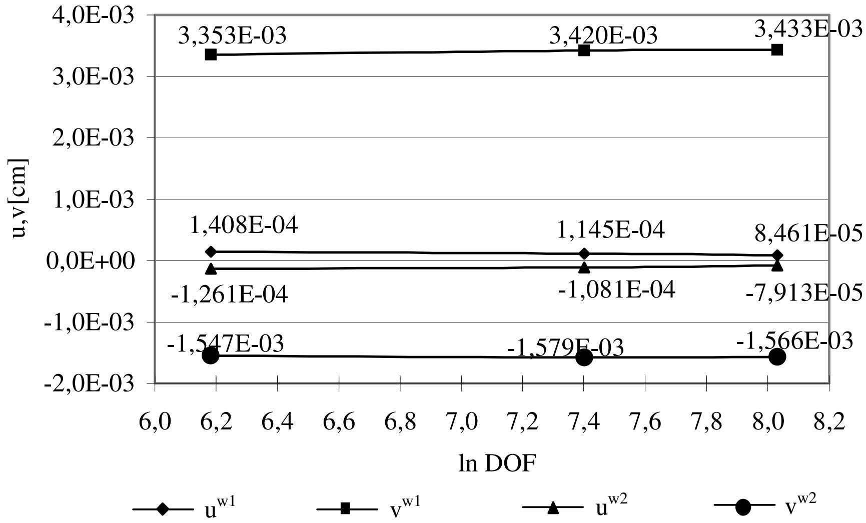

Fig. 8. Displacements of points w1, w2 of REO_I for various meshes, load case 2

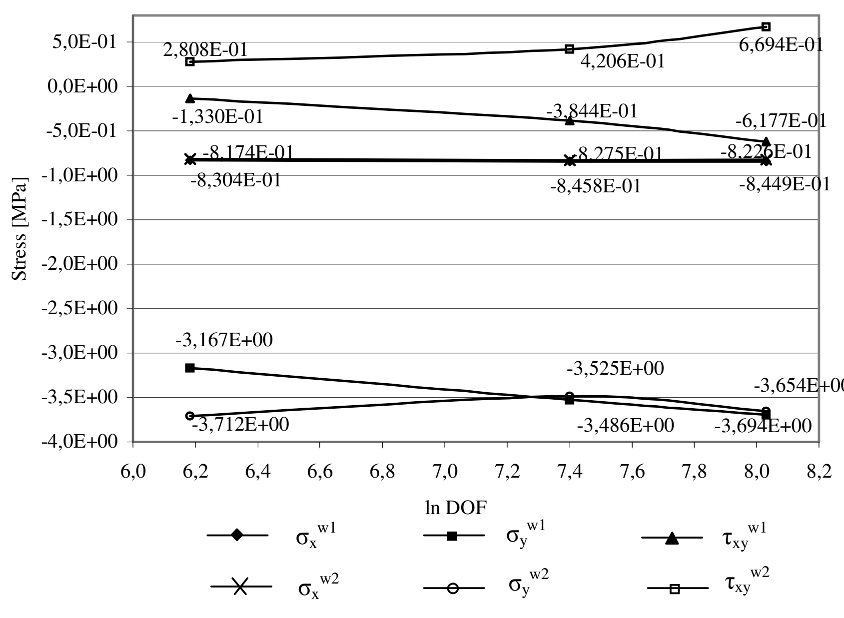

Fig. 9. Stresses at points w1 and w2 of REO_I for various meshes, load case 2

Distributions of stresses along characteristic cross-sections for various meshes are shown in figs. 10 to 13. As can be observed, these solutions exhibit good convergence properties. All the graphs in figs. 8 to 14 correspond to the load case 2.

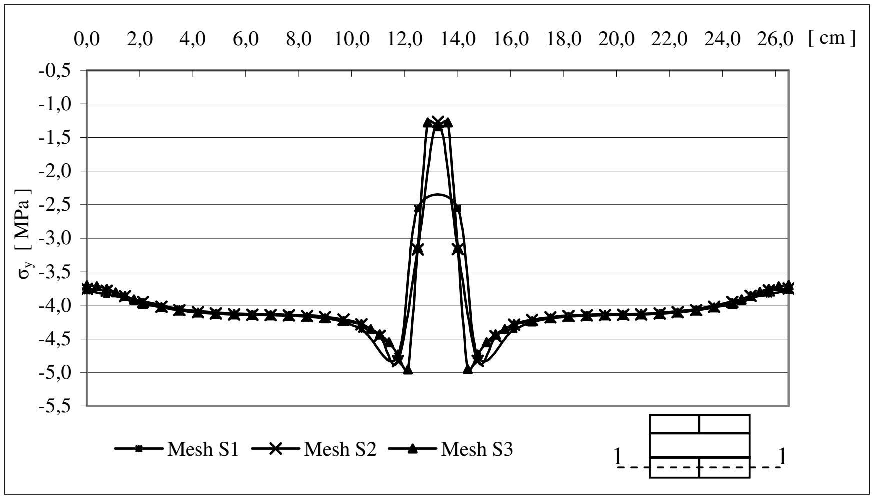

Fig. 10. Stress σ_y in REO_I along section 1-1 for various meshes, load case 2

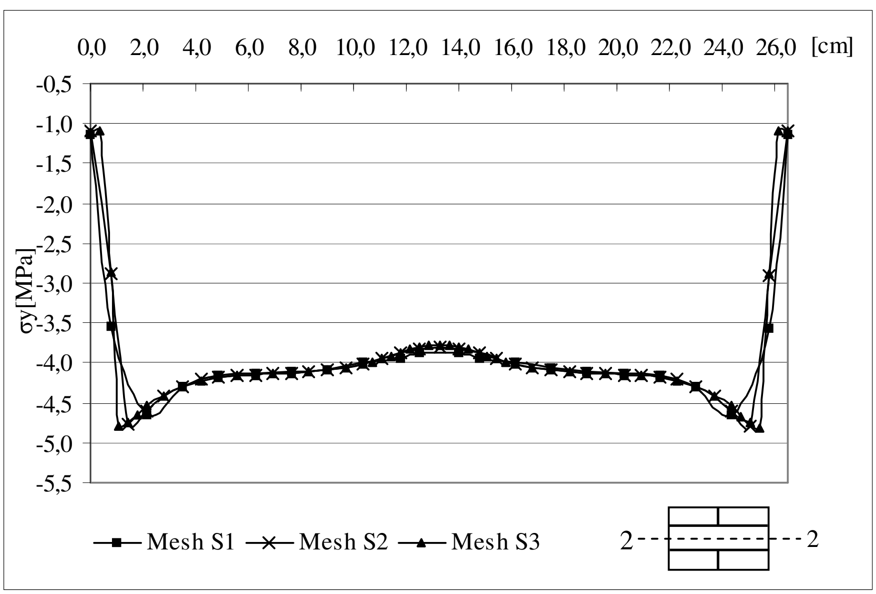

Fig. 11. Stress σ_y in REO_I along section 2-2 for various meshes, load case 2

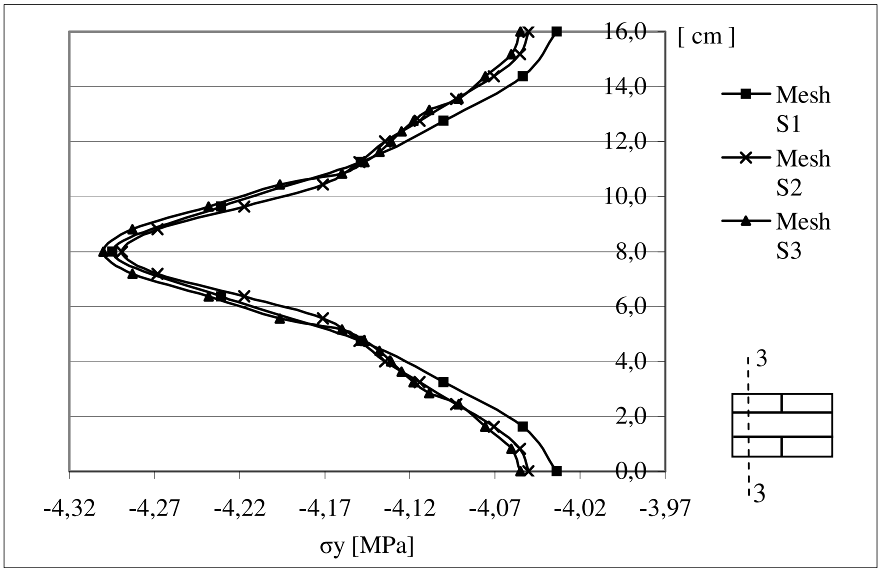

Fig. 12. Stress σ_y in REO_I along section 3-3 for various meshes, load case 2

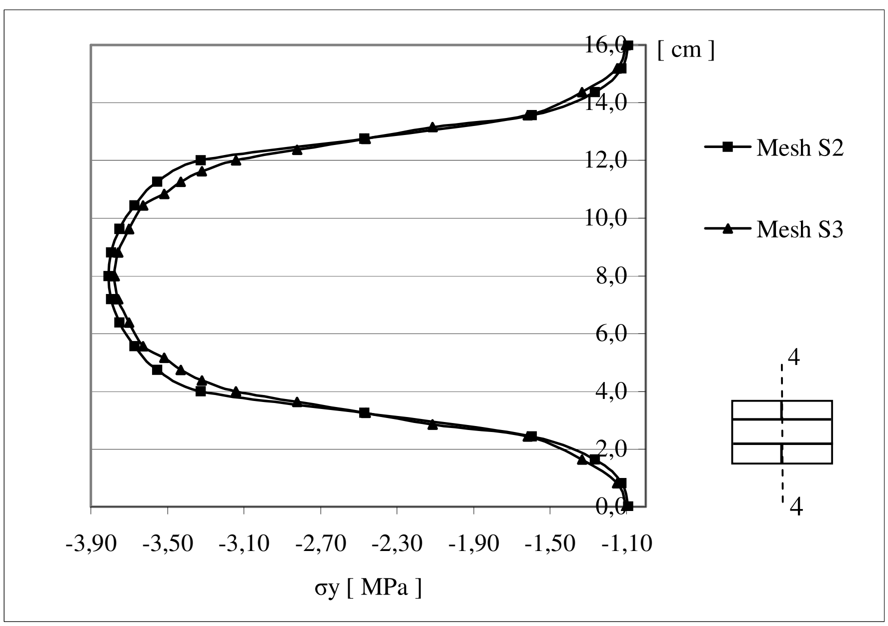

Fig. 13. Stress σ_y in REO_I along section 4-4 for various meshes, load case 2

Averaged values of stresses $\bar{\boldsymbol{\sigma}}$ and strains $\bar{\boldsymbol{\varepsilon}}$ for masonry cells REO and MUR, can be calculated component wise according formula (1) and are collected in tab. 2 for the three load cases.

Table 2. Averaged stresses and strains for cells REO and MUR

Load case 1 $\bar{\tau}_{xy}, \bar{\varepsilon}_y, \bar{\gamma}_{xy} = 0$				
Cell	Mesh	$\bar{\sigma}_x$ [MPa]	$\bar{\sigma}_y$ [MPa]	$\bar{\varepsilon}_x$
REO_I	S1	-2.7941	-0.4446	-3.7736E-04
	S2	-2.5772	-0.4156	-3.7736E-04
	S3	-2.5134	-0.3949	-3.7736E-04
REO_II	S1	-2.7941	-0.4446	-3.7736E-04
	S2	-2.5772	-0.4156	-3.7736E-04
	S3	-2.5134	-0.3949	-3.7736E-04
MUR_I	M1	-2.7716	-0.4344	-3.7736E-04
MUR_II	M1	-2.7714	-0.4340	-3.7736E-04
Load case 2 $\bar{\tau}_{xy}, \bar{\varepsilon}_x, \bar{\gamma}_{xy} = 0$				
Cell	Mesh	$\bar{\sigma}_x$ [MPa]	$\bar{\sigma}_y$ [MPa]	$\bar{\varepsilon}_y$
REO_I	S1	-0.8140	-4.0127	-6.2500E-04
	S2	-0.8237	-4.0042	-6.2500E-04
	S3	-0.8267	-4.0009	-6.2500E-04
REO_II	S1	-0.8140	-4.0127	-6.2500E-04
	S2	-0.8237	-4.0042	-6.2500E-04
	S3	-0.8267	-4.0009	-6.2500E-04
MUR_I	M1	-0.8160	-4.0078	-6.2500E-04
MUR_II	M1	-0.8160	-4.0078	-6.2500E-04

Load case 3 $\bar{\sigma}_x, \bar{\sigma}_x, \bar{\varepsilon}_x, \bar{\varepsilon}_y = 0$			
Cell	Mesh	$\bar{\tau}_{xy}$ [MPa]	$\bar{\gamma}_{xy}$
REO_I	S1	2.4069	5.6166E-04
	S2	2.5456	5.8668E-04
	S3	2.5338	5.8686E-04
REO_II	S1	2.4523	5.5334E-04
	S2	2.5993	5.8111E-04
	S3	2.5930	5.8095E-04
MUR_I	M1	2.5102	5.9724E-04
MUR_II	M1	2.5428	5.9600E-04

We can determine the effective material parameters of masonry as an equivalent homogeneous orthotropic material by formulae [4]:

$$\overline{\nu}_y = \overline{\sigma}_x^{(2)} / \overline{\sigma}_y^{(2)}, \quad \overline{\nu}_x = \overline{\sigma}_y^{(1)} / \overline{\sigma}_x^{(1)} \tag{11}$$

$$\overline{E}_x = \overline{\sigma}_x^{(1)} (1 - \overline{\nu}_x \overline{\nu}_y) / \overline{\varepsilon}_x^{(1)} = \left(\overline{\sigma}_x^{(1)} (1 - \frac{\overline{\sigma}_x^{(2)}}{\overline{\sigma}_y^{(2)}} \frac{\overline{\sigma}_y^{(1)}}{\overline{\sigma}_x^{(1)}}) / \overline{\varepsilon}_x^{(1)} \right) \tag{12}$$

$$\overline{E}_y = \overline{\sigma}_y^{(2)} (1 - \overline{\nu}_x \overline{\nu}_y) / \overline{\varepsilon}_y^{(2)} = \left(\overline{\sigma}_y^{(2)} (1 - \frac{\overline{\sigma}_x^{(2)}}{\overline{\sigma}_y^{(2)}} \frac{\overline{\sigma}_y^{(1)}}{\overline{\sigma}_x^{(1)}}) / \overline{\varepsilon}_y^{(2)} \right) \tag{13}$$

$$\overline{G} = \overline{\tau}_{xy}^{(3)} / \overline{\gamma}_{xy}^{(3)} \tag{14}$$

in which the super index $^{(i)}$ indicates the number of corresponding load case.
Table 3 contains the obtained values of effective material parameters according to eqns. (11) –(14) for values of stresses and strains given in tab. 2.

Table 3. Effective parameters for masonry calculated for various cells

Cell	Mesh	$\overline{E}_x$ [MPa]	$\overline{E}_y$ [MPa]	$\overline{\nu}_x$	$\overline{\nu}_y$	$\overline{G}$ [MPa]
REO_I 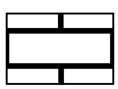	**S1**	7165	6213	0.1591	0.2028	4285
	S2	6603	6194	0.1613	0.2057	4339
	S3	6444	6193	0.1571	0.2066	4318
REO_II 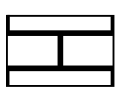	**S1**	7165	6213	0.1591	0.2028	4432
	S2	6603	6194	0.1613	0.2057	4473
	S3	6444	6193	0.1571	0.2066	4463
MUR_I	**M1**	7110.2	6207.9	0.1567	0.2036	4203.0
MUR_II	**M1**	7110.3	6208.1	0.1566	0.2036	4266.3

The final results of tab. 3 show that the values of parameters dependent on the coarseness of finite element meshes applied but are independent of representative cells used, the existing differences for small REO and bigger MUR cells seem to be an effect of relative coarseness of meshes applied to MUR cells. It is remarkable that the Young modulus $\overline{E}_x$ has appeared most sensitive (10 %), whilst $\overline{E}_y$ least sensitive (0.3 %) and both approaching different values.

5. ELASTIC MODULUS BY OTHER RESERCHES

There are proposed many formulae for determination of material parameters for masonry in the literature. These formulae usually do not account for anisotropic properties of masonry, but rather treat it as an isotropic material with, for example, Kirchhoff's modulus G is usually estimated as 40% E [10].

By Polish Standard: PN-B-03002 „Unreinforced masonry structures", the elastic modulus E of masonry can be calculated as

$$E = \alpha_c f_k \tag{15}$$

where f_k is compressive strength of masonry and α_c is a coefficient. For brick masonry and for mortar with compressive strength $f_m \leq 5$ MPa, one can assume $\alpha_c = 600$. Compressive strength of masonry can be calculated as

$$f_k = K\ f_b^{0,65} f_m^{0,25} \tag{16}$$

where K is a coefficient dependent on element group [9], f_b and f_m is respectively compressive strength of brick and mortar. For the first element group and for compressive strength of brick $f_b > 40$ MPa, one can take K = 0.55.

Hendry [5] gives a similar formula,

$$E = 700\ \sigma_c^{'} \tag{17}$$

where $\sigma_c^{'}$ is compressive strength of masonry.

The next two formulae account for elastic moduli of brick E_b and mortar E_m. Matysek [6] has proposed the following expression

$$E = \frac{1,25\xi + 1}{1,25\xi + \beta} E_b \tag{18}$$

in which ξ is the ratio of brick's height to thickness of mortar joint and β is the ratio of brick's elastic modulus to that of mortar. Another formula was suggested by Brooks [6]

$$\frac{1}{E} = \frac{0{,}86}{E_b} + \frac{0{,}14}{E_m} \tag{19}$$

According to Ciesielski [3], the elastic modulus can be obtained as

$$E^i_{śr} = \frac{1{,}20\, E^i_b\, E^i_m}{0{,}20 E^i_b + E^i_m} \tag{20}$$

where E^i_b, E^i_m are medium elastic moduli of brick and mortar in section i.

Values of elastic modulus determined according to suggestions (15) – (20) and material data given in table 1 are collected in table 4.

Table 4. Elastic modulus of masonry

Author	Elastic modulus *E* [MPa]
PN-B-03002	6087
Ciesielski	6600
Matysek	6776
Hendry	7000
Brooks	7051

It may be noted that the values of elastic modulus obtained by proposals of other researches are similar to the results obtained in our numerical simulations.

6. CONCLUSION

In this paper we have presented a numerical homogenization technique for determination of effective elastic material parameters of brick masonry. The applied approach is based on the finite element method which is used for discretization of the corresponding boundary value problem posed on a representative cell of masonry for three particalar loading cases.

The obtained numerical results confirm the orthotropic properties of brick masonry. The calculated Young moduli in horizontal direction is larger than the one in vertical direction. This is also observed in laboratory tests by other reserches. In fact, we have considered different representative masonry cells (REO_I, REO_II, MUR_I, MUR_II) and the obtained results are practically the same, as expected. Some noticable differeces are observed for different finness of finite element meshes.

Numerical simulation has proved to be a convenient powerful tool for homogenization of masonry material, and should be regarded as the effective complementary tool to laboratory tests. The values of material parameters determined herein by means of numerical homogenization can further be used as input to an elastic homogeneous model of large-scale masonry structures.

REFERENCES

1. Anthoine A., *Derivation of the in-plane elastic characteristics of masonry through homogenization theory*, Int. J. Solids Struct. **32**, 2 (1995), 137-163.
2. Bull J. W. (Ed.), *Computational modeling of masonry, brickwork and block-work structures*, Saxe-Coburg Publications, Dun Eaglais 2001.
3. Ciesielski R., *„O dynamicznych modułach sprężystości murów z cegły”,* XLV Konferencja Naukowa Wrocław – Krynica, 1999, 117-124.
4. Guowei Ma, Hong Hao, Member, ASCE, Yong Lu: *Homogenization of masonry using numerical simulations*, Journal of Engineering Mechanics **127**, 2001, 421-431.
5. Hendry A. W., Sinha B. P., Davies S. R., *Design of masonry structures*, E&FN SPON, London 1997.
6. Kubica J., Drobiec Ł., Jasiński R., *Badania siecznego modułu sprężystości murów z cegły*, XLV Konferencja Naukowa, Wrocł.–Krynica 1999, 133-140.
7. Lopez J., Oller S., Onate E., Lubliner J.: *Homogeneous constitutive model for masonry*, Int. J. Numer. Meth. Engng. **46**, 1999, 1651-1671.
8. T. Łodygowski, M. Wierszycki, *Zastosowanie homogenizacji numerycznej muru ceglanego do oceny nośności złożonych konstrukcji*, VI Konferencja Naukowa Konstrukcje Zespolone, Zielona Góra 2002, 79-102.
9. W. Starosolski, R. Kliszczewicz, J. Kubica, *Badania żelbetowych modeli ram żelbetowych wypełnionych murami z drobnowymiarowych elementów*, Prace Instytutu Techniki Budowlanej, **1-2**, 1991, 96-105.
10. Zienkiewicz O.C: *Metoda elementów skończonych*, Arkady, Warszawa 1972.
11. PN-B-03002:1999, Konstrukcje murowe niezbrojone.
12. ENV 1996-1-1:1995, *EUROKOD 6*: Projektowanie konstrukcji murowych, część 1-1: Reguły ogólne. Reguły dla murów niezbrojonych, zbrojonych i sprężonych.

Acknowledgements. Work supported by the Committee for Scientific Research (KBN) under Grant No. 5 T07A 042 24 in the years 2003-2006. This support is gratefully acknowledged.

NUMERYCZNA HOMOGENIZACJA SPRĘŻYSTYCH ŚCIAN CEGLANYCH

S t r e s z c z e n i e

Praca dotyczy numerycznego sposobu homogenizacji muru ceglanego w zakresie sprężystym. Problem homogenizacji postawiono w płaskim stanie naprężenia. Odpowiednie zagadnienie brzegowe na reprezentatywnej komórce zdyskretyzowano metodą elementów skończonych wykorzystując czterowęzłowy element skończony o ośmiu stopniach swobody i opracowany własny program komputerowy. Zastosowana metoda homogenizacji pozwala wyznaczyć dla muru, który jest niejednorodnym dwuskładnikowym materiałem kompozytowym, wartości pieciu efektywnych parametrów materiałowych dla jednorodnego materiału ortotropowego. Wyznaczone parametry mogą następnie być użyte w analizach całych, dużych konstrukcji murowych. Otrzymane wyniki analiz numerycznych porównano z propozycjami obliczania modułu sprężystości muru według innych badaczy, uzyskując dobrą zgodność jakościową.

APPENDIX

We list here formulae for the entries K_{ij} of the elemental stiffness matrix $\mathbf{K}^e$ for the orthotropic four-node quadrilateral finite element with eight degrees of freedom. By a and b we denote here the dimensions of the element respectively along axis x and y, and g stands for its thickness.

$$\mathbf{K}^e = g \int_{\Omega^e} \mathbf{B}^T \mathbf{D}\, \mathbf{B} d\Omega = g \int_0^a \int_0^b \mathbf{B}^T \mathbf{D} \mathbf{B}\, d\tilde{x} d\tilde{y}$$

$$K_{ij} = K_{ji}, \qquad \alpha = a/b, \qquad \beta = b/a, \qquad \mathbf{D} = \begin{bmatrix} d_{11} & d_{12} & 0 \\ d_{21} & d_{22} & 0 \\ 0 & 0 & d_{33} \end{bmatrix}$$

$$K_{11} = \frac{g}{3}(\beta d_{11} + \alpha d_{33}); K_{12} = \frac{g}{4}(d_{12} + d_{33}); K_{13} = -\frac{g}{6}(2\beta d_{11} - \alpha d_{33})$$

$$K_{14} = \frac{g}{4}(d_{12} - d_{33}); K_{15} = -\frac{g}{6}(\beta d_{11} + \alpha d_{33}); K_{16} = -\frac{g}{4}(d_{12} + d_{33})$$

$$K_{17} = \frac{g}{6}(\beta d_{11} - 2\alpha d_{33}); K_{18} = \frac{g}{4}(-d_{12} + d_{33})$$

$$K_{22} = \frac{g}{3}(\alpha d_{22} + \beta d_{33}); K_{23} = \frac{g}{4}(-d_{21} + d_{33}); K_{24} = \frac{g}{6}(\alpha d_{22} - 2\beta d_{33})$$

$$K_{25} = -\frac{g}{4}(d_{21} + d_{33})\,;\ K_{26} = -\frac{g}{6}(\alpha d_{22} + \beta d_{33})\,;\ K_{27} = \frac{g}{4}(d_{21} - d_{33})$$

$$K_{28} = -\frac{g}{6}(2\alpha d_{22} - \beta d_{33})\,;\ K_{33} = \frac{g}{3}(\beta d_{11} + \alpha d_{33})\,;\ K_{34} = -\frac{g}{4}(d_{12} + d_{33})\,;$$

$$K_{35} = \frac{g}{6}(\beta d_{11} - 2\alpha d_{33})\,;\ K_{36} = \frac{g}{4}(d_{12} - d_{33})\,;\ K_{37} = -\frac{g}{6}(\beta d_{11} + \alpha d_{33})\,;$$

$$K_{38} = \frac{g}{4}(d_{12} + d_{33})\,;\ K_{44} = \frac{g}{3}(\alpha d_{22} + \beta d_{33})\,;\ K_{45} = \frac{g}{4}(-d_{21} + d_{33})\,;$$

$$K_{46} = -\frac{g}{6}(2\alpha d_{22} - \beta d_{33})\,;\ K_{47} = \frac{g}{4}(d_{21} + d_{33})\,;\ K_{48} = -\frac{g}{6}(\alpha d_{22} + \beta d_{33})$$

$$K_{55} = \frac{g}{3}(\beta d_{11} + \alpha d_{33})\,;\ K_{56} = \frac{g}{4}(d_{12} + d_{33})\,;\ K_{57} = -\frac{g}{6}(2\beta d_{11} - \alpha d_{33})$$

$$K_{58} = \frac{g}{4}(d_{12} - d_{33})\,;\ \mathrm{K}_{66} = \frac{g}{3}(\alpha \mathrm{d}_{22} + \beta \mathrm{d}_{33})\,;\ K_{67} = \frac{g}{4}(d_{33} - d_{21})\,;$$

$$K_{68} = \frac{g}{6}(\alpha d_{22} - 2\beta d_{33})\,;\ K_{77} = \frac{g}{3}(\beta d_{11} + \alpha d_{33})\,;\ K_{78} = -\frac{g}{4}(d_{12} + d_{33})$$

$$K_{88} = \frac{g}{3}(\alpha d_{22} + \beta d_{33})$$